

## A Strong Atlantic Meridional Mode Event in 2009: The Role of Mixed Layer Dynamics\*

GREGORY R. FOLTZ

*NOAA/Atlantic Oceanographic and Meteorological Laboratory, Miami, Florida*

MICHAEL J. MCPHADEN

*NOAA/Pacific Marine Environmental Laboratory, Seattle, Washington*

RICK LUMPKIN

*NOAA/Atlantic Oceanographic and Meteorological Laboratory, Miami, Florida*

(Manuscript received 9 March 2011, in final form 30 June 2011)

### ABSTRACT

In the first half of 2009, anomalous cooling of sea surface temperatures (SSTs) in the equatorial North Atlantic (ENA; 2°–12°N) triggered a strong Atlantic meridional mode event. During its peak in April–May, SSTs in the ENA were 1°C colder than normal and SSTs in the equatorial South Atlantic (5°S–0°) were 0.5°C warmer than normal. Associated with the SST gradient were anomalous northerly winds, an anomalous southward shift of the intertropical convergence zone, and severe flooding in Northeast Brazil. This study uses in situ and satellite observations to examine the mechanisms responsible for the anomalous cooling in the ENA during boreal winter and spring of 2009. It is found that the cooling was initiated by stronger than normal trade winds during January and February 2009 associated with an anomalous strengthening of the subtropical North Atlantic high pressure system. Between 6° and 12°N, unusually strong trade winds cooled the ocean through wind-induced evaporation and deepened the mixed layer anomalously by 5–20 m. Closer to the equator, surface equatorial winds responded to the anomalous interhemispheric SST gradient, becoming northwesterly between the equator and 6°N. The anomalous winds drove upwelling of 0.5–1 m day<sup>-1</sup> during March–April, a period when there is normally weak downwelling. The associated vertical turbulent heat flux at the base of the mixed layer led to unusually cool SSTs in the central basin, further strengthening the anomalous interhemispheric SST gradient. These results emphasize the importance of mixed layer dynamics in the evolution of the meridional mode event of 2009 and the potential for positive coupled feedbacks between wind-induced upwelling and SST in the ENA.

### 1. Introduction

Interannual to decadal variability in the tropical Atlantic is influenced by the Atlantic meridional mode (AMM), characterized by an anomalous meridional gradient of sea surface temperature (SST) between the tropical North and South Atlantic (Nobre and Shukla 1996). Anomalously warm SSTs in the tropical North

Atlantic relative to the South Atlantic are associated with anomalous southerly surface winds and a northward anomalous displacement of the intertropical convergence zone (ITCZ). Conversely, anomalously cold SSTs in the North Atlantic relative to the South Atlantic are associated with anomalous northerly winds and a southward shift of the ITCZ. The AMM exerts a strong influence on rainfall in Northeast Brazil and the Sahel, since rainfall in these regions is closely linked to the seasonal movement of the ITCZ (Lamb 1978; Hastenrath and Greischar 1993; Giannini et al. 2003). The AMM tends to peak in boreal spring, when SST variability in the tropical North Atlantic is strongest and the ITCZ is most sensitive to anomalies in the meridional gradient of SST (Chiang et al. 2002; Xie and Carton 2004; Hu and Huang 2006).

\* Pacific Marine Environmental Laboratory Publication 3673.

Corresponding author address: Gregory R. Foltz, 4301 Rick-enbacker Cswy., NOAA/AOML, Miami, FL 33149.  
E-mail: gregory.foltz@noaa.gov

An important step toward understanding the coupled variability of the AMM is to understand what drives SST variability associated with this mode. Interannual variability of SST in the tropical Atlantic is strongest in the northeastern basin ( $2^{\circ}$ – $20^{\circ}$ N,  $15^{\circ}$ – $40^{\circ}$ W) and in the eastern equatorial Atlantic, in connection with the AMM and Atlantic Niños, respectively (Huang et al. 2004). SST variability in the tropical North Atlantic (TNA;  $12^{\circ}$ – $25^{\circ}$ N) is driven primarily by changes in wind-induced latent heat loss (Carton et al. 1996). The surface wind variability itself is influenced by the North Atlantic Oscillation (NAO) and atmospheric teleconnections from the eastern equatorial Pacific (Enfield and Mayer 1997; Czaja et al. 2002). Changes in shortwave radiation (SWR) from low-level cloudiness and African dust appear to play an important secondary role (Tanimoto and Xie 2002; Foltz and McPhaden 2008). In contrast, relatively little is known about what drives SST variability in the equatorial North Atlantic (ENA;  $2^{\circ}$ – $12^{\circ}$ N), which underlies the mean position of the ITCZ. This is a region with climatologically warm SSTs [ $27^{\circ}$ C, averaged during March–May (MAM) over  $2^{\circ}$ – $12^{\circ}$ N,  $10^{\circ}$ – $50^{\circ}$ W] where SST anomalies are likely to have a significant influence on atmospheric circulation and rainfall, and hence the AMM (e.g., Chang et al. 2001). Modeling studies suggest that ocean dynamics play an important role in this region (Carton and Huang 1994; Carton et al. 1996). However, there is very little direct observational evidence to support this hypothesis, and it is unclear which oceanic processes might be important.

In 2009 there was a strong negative AMM event that was initiated by anomalous cooling in the TNA. The cold SST anomalies during January and February 2009 coincided with a moderate La Niña in the equatorial Pacific, stronger than normal convection in the Amazon, and an anomalously strong North Atlantic subtropical high pressure system, all of which are consistent with enhanced trade winds and cooler than normal SSTs in the TNA. The coldest SST anomalies shifted southward to the ENA during February and March 2009. The AMM peaked shortly thereafter in March–May, when surface winds in the tropical Atlantic are most sensitive to the cross-equatorial gradient of SST and the positive wind evaporation–SST feedback is strongest (Chang et al. 1997; Chiang et al. 2002; Xie and Carton 2004). By one measure, the anomalous meridional SST gradient in the boreal spring of 2009 was the strongest since satellite SST measurements began in 1982 (Foltz and McPhaden 2010a; Fig. 1). The SST gradient and its associated surface wind anomalies drove a southward displacement of the ITCZ, contributing to severe flooding in Northeast Brazil (Figs. 1b,c). The surface wind anomalies forced equatorial Rossby waves, which reflected from the western

boundary and caused abrupt anomalous cooling of the equatorial cold tongue in the summer of 2009 (Foltz and McPhaden 2010a). Cold SST anomalies in the TNA persisted into the boreal summer of 2009, conspiring with a developing Pacific El Niño to produce below-normal tropical cyclone activity (nine tropical cyclones developed in the Atlantic during 2009, the fewest since 1997). The low activity in 2009 is consistent with previous analyses showing that the Atlantic hurricane season is influenced by the state of the equatorial Pacific and SSTs in the TNA (Wang et al. 2006; Latif et al. 2007).

In the past several years there have been substantial improvements to the long-term observational network in the tropical Atlantic Ocean. The global array of Argo floats reached completion in the mid-2000s (Gould et al. 2004), and four Prediction and Research Moored Array in the Tropical Atlantic (PIRATA) buoys were deployed as part of the Northeast Extension in 2006–07 (Bourlès et al. 2008). In this study we use these relatively new measurements, together with ongoing satellite observations, to analyze the causes of the anomalous cooling in the North Atlantic ( $2^{\circ}$ – $25^{\circ}$ N) in 2009. This region is chosen because of the strong anomalies here that were well sampled by in situ observations (Fig. 2). In comparison, SST anomalies in the South Atlantic were weaker, and in situ observations were sparser.

The rest of the paper is organized as follows. We first describe the datasets used. The evolution of the SST anomalies is then presented in relation to surface wind and subsurface ocean anomalies. The mixed layer temperature balance is analyzed using Argo and satellite data and compared to results from two PIRATA moorings. Finally, the results are summarized and discussed.

## 2. Data

A combination of satellite, in situ, and atmospheric reanalysis datasets is used to examine the evolution of anomalous conditions in the tropical Atlantic during 2009 and to analyze the mixed layer temperature budget.

### a. Satellite data, reanalysis fields, and Argo

The satellite datasets consist of SST, surface winds, and outgoing longwave radiation (OLR). SST is available from the Tropical Rainfall Measuring Mission (TRMM) Microwave Imager (TMI) and the Advanced Microwave Scanning Radiometer for Earth Observing System (AMSR-E). These data are blended together using optimal interpolation and are available as daily averages on a  $0.25^{\circ} \times 0.25^{\circ}$  grid from June 2002 to the present from Remote Sensing Systems (<ftp://discover-earth.org/sst>). We have averaged these data to a  $1^{\circ} \times 1^{\circ}$  spatial resolution for consistency with the velocity and surface heat flux

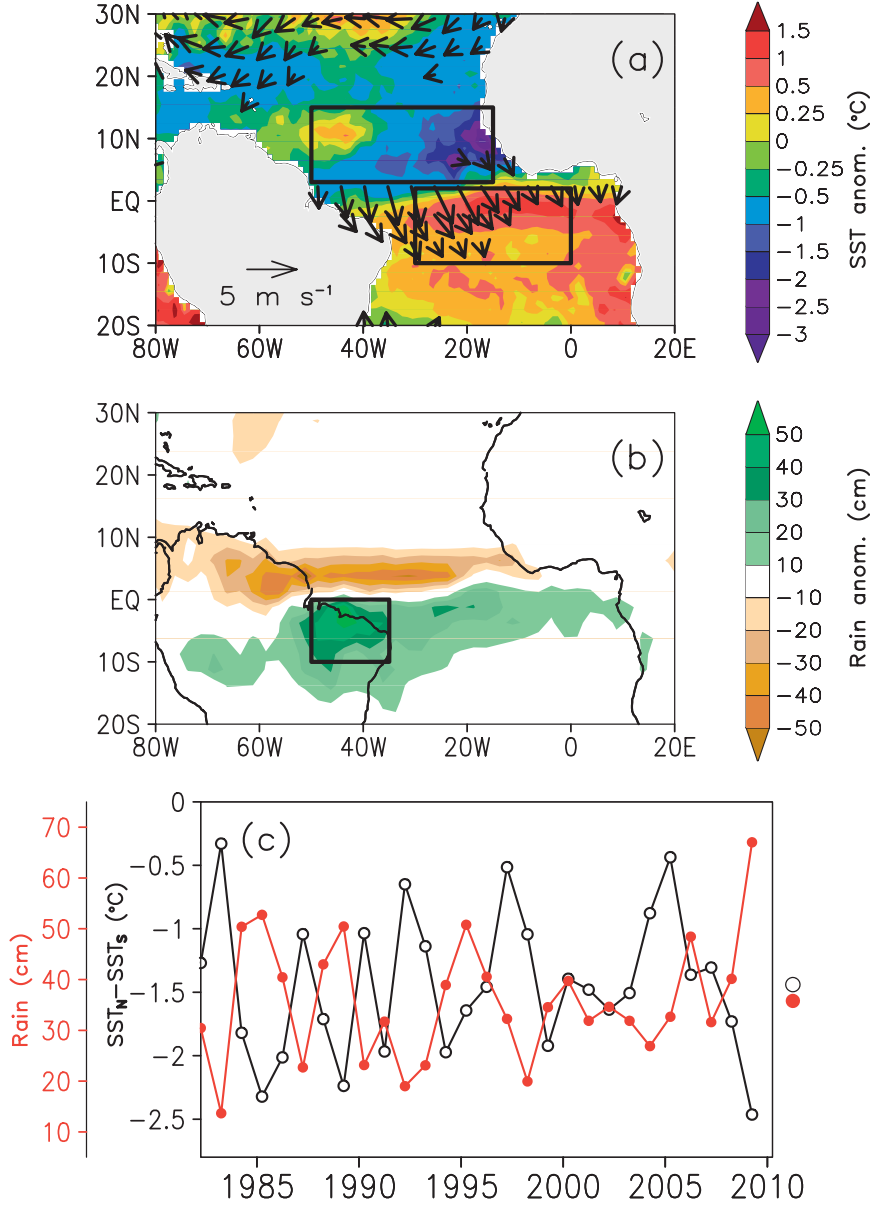


FIG. 1. (a) Interannual anomalies of TMI-AMSR-E SST (shaded) and QuikSCAT wind velocity (vectors) averaged during April–May 2009. Wind vectors are plotted only where the magnitude of the wind speed anomaly is  $>1 \text{ m s}^{-1}$ . (b) As in (a), but shading indicates GPCP rainfall anomaly. Here and in subsequent figures, anomalies are with respect to the 2003–08 monthly mean seasonal cycle unless otherwise indicated. (c) Meridional SST gradient index (black line) averaged during April–May, calculated as the Reynolds et al. (2002) SST anomaly averaged in the tropical North Atlantic minus South Atlantic [regions are indicated by boxes in (a)], and April–May Northeast Brazil rainfall (red line), calculated from GPCP averaged in boxed region shown in (b). Note that in (c) the values for each year include the record-length mean and are not anomalies as in (a) and (b). Black circle and red dot on the right in (c) are the record-length means of meridional SST gradient index and Northeast Brazil rainfall, respectively.

datasets described later in this section. Surface wind velocity from the SeaWinds instrument on the Quick Scatterometer (QuikSCAT) satellite is available from Institut Français de Recherche pour l'exploitation de la Mer

(IFREMER)/Centre ERS d'Archivage et de Traitement (CERSAT) on a  $0.5^\circ \times 0.5^\circ$  daily grid from July 1999 to November 2009 (<ftp://ftp.ifremer.fr/ifremer/cersat/products/gridded/mwf-quikscat>). Wind stress is calculated

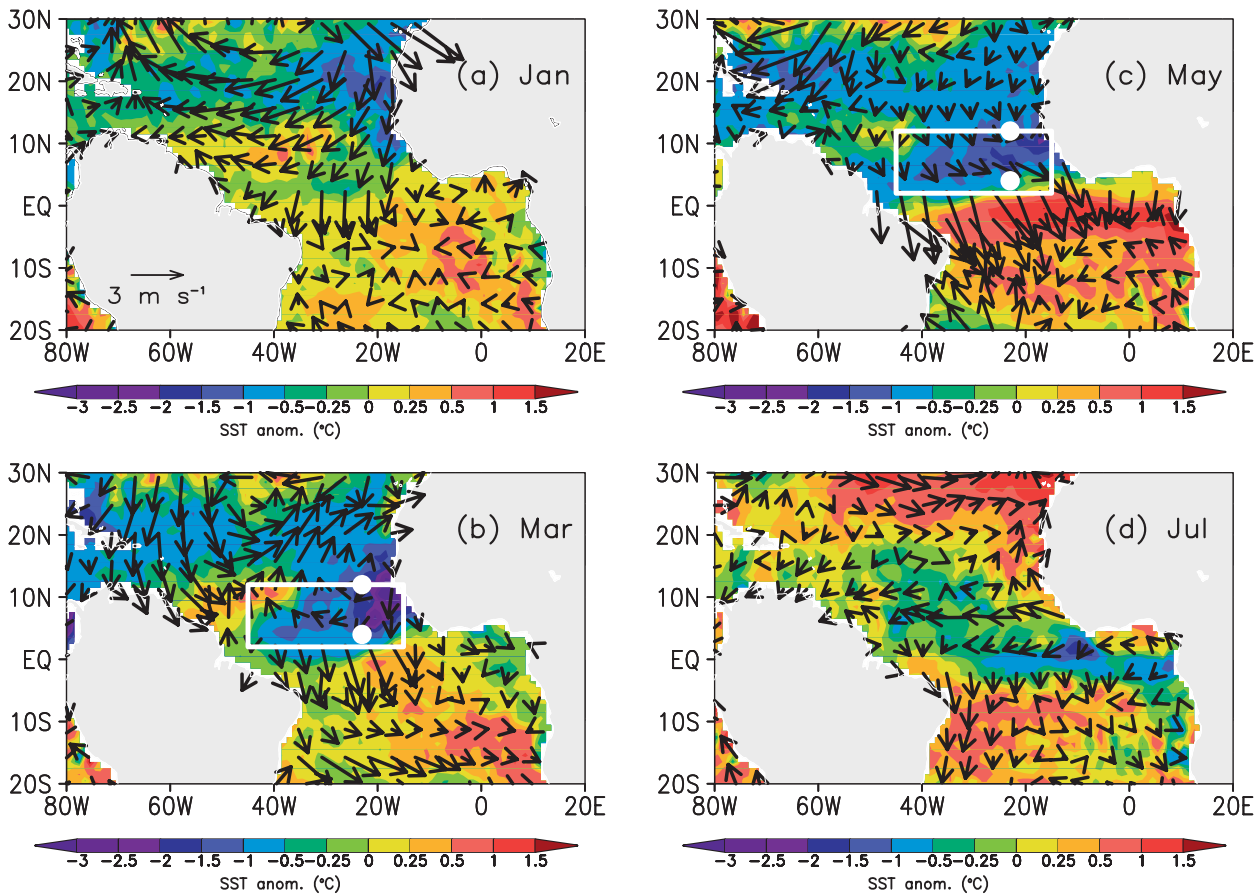


FIG. 2. Interannual anomalies of SST (shaded) and surface wind velocity (vectors) during 2009 for the months of (a) January, (b) March, (c) May, and (d) July. White boxes in (b) and (c) indicate the equatorial North Atlantic (ENA) region used for temperature budget analysis. White dots in (b) and (c) are the positions of the PIRATA moorings used in this study.

using a constant drag coefficient of  $1.5 \times 10^{-3}$  and an air density of  $1.29 \text{ kg m}^{-3}$ . The National Oceanic and Atmospheric Administration (NOAA) interpolated OLR, available on a  $2.5^\circ \times 2.5^\circ$  grid for 1979–present, is used to detect regions of atmospheric deep convection (Liebmann and Smith 1996).

Horizontal currents averaged in the upper 30 m are available from the Ocean Surface Current Analysis–Real-time (OSCAR; Bonjean and Lagerloef 2002). This product uses satellite sea level, wind stress, and SST, together with a diagnostic model, to calculate velocity on a  $1^\circ \times 1^\circ$  grid every five days for the period 1993–present.

We also use combined satellite/in situ datasets of SST and precipitation. Monthly optimally interpolated SST is available on a  $1^\circ \times 1^\circ$  grid from December 1981 to the present (Reynolds et al. 2002). The Global Precipitation Climatology Project (GPCP) provides monthly mean precipitation from January 1979 to the present on a  $2.5^\circ \times 2.5^\circ$  grid (Adler et al. 2003; <http://www.cdc.noaa.gov/cdc/data.gpcp.html>). These datasets are used to put the 2009 anomalies into perspective with the longer-term

variability in the tropical Atlantic (Fig. 1). We also use daily surface atmospheric pressure, air temperature, and specific humidity from the National Centers for Environmental Prediction (NCEP)–National Center for Atmospheric Research (NCAR) reanalysis for the time period 1982–2009 on a  $2^\circ \times 2^\circ$  grid (Kalnay et al. 1996). The surface pressure data are used to calculate atmospheric indices during 2008–09 (Table 1). The air temperature and specific humidity data are combined with QuikSCAT wind speed and TMI–AMSR-E SST to calculate surface latent and sensible heat loss using version 3 of the Coupled Ocean–Atmosphere Response Experiment (COARE) bulk flux algorithm (Fairall et al. 2003). This hybrid satellite–reanalysis approach is used because of significant errors in the reanalysis wind speed and turbulent heat fluxes (e.g., Sun et al. 2003). Surface shortwave radiation and net longwave emission are obtained from the TropFlux (see <http://www.lodyc.jussieu.fr/tropflux/index.html>) analysis on a  $1^\circ \times 1^\circ$  daily grid for 1989–2009 (Kumar et al. 2011). This product calculates surface shortwave radiation by combining

TABLE 1. Climatic indices during December 2007–March 2008 and December 2008–March 2009. All values are monthly anomalies with respect to the corresponding 1982–2009 monthly means, normalized by the standard deviation. Tropical North Atlantic (TNA) wind speed is averaged over 5°–20°N, 15°–50°W. NAO index is NCEP–NCAR reanalysis surface pressure at the Azores minus Iceland. The Niño-3.4 index is SST averaged over 5°S–5°N, 120°–170°W. The subtropical high (STH) index is NCEP–NCAR reanalysis surface pressure averaged over 20°–25°N, 30°–40°W. The Amazon convection index (Amzn) is satellite OLR averaged over 10°S–5°N, 30°–70°W. Negative values of OLR indicate enhanced convection. Bold font highlights the months with the strongest positive wind speed anomalies in the TNA in 2009.

	TNA WS	Niño-3.4	NAO	STH	Amzn
2007/08					
Dec	0.2	-1.2	0.5	-0.3	-1.0
Jan	<b>-0.4</b>	<b>-1.4</b>	<b>0.4</b>	<b>-1.1</b>	<b>0.1</b>
Feb	<b>0.0</b>	<b>-1.8</b>	<b>-0.1</b>	<b>-0.5</b>	<b>-0.3</b>
Mar	-0.7	-1.4	0.3	-1.2	-1.2
2008/09					
Dec	-1.0	-0.7	-0.2	-1.2	-0.9
Jan	<b>2.2</b>	<b>-0.7</b>	<b>0.9</b>	<b>1.5</b>	<b>-0.4</b>
Feb	<b>1.6</b>	<b>-0.7</b>	<b>-0.6</b>	<b>0.3</b>	<b>-0.9</b>
Mar	-0.2	-0.6	0.1	-1.8	-0.2

a satellite-based product (Zhang et al. 2004) with satellite outgoing longwave radiation. Net surface longwave radiation (LWR) in TropFlux is calculated from the European Centre for Medium-Range Weather Forecasts (ECMWF) reanalysis after bias and amplitude correction.

Monthly averaged mixed layer depth, thermocline depth, and the temperature 10 m below the mixed layer are computed using temperature and salinity profiles from Argo floats during 2005–09, when the coverage in the tropical Atlantic is highest. The vertical resolution of the temperature and salinity profiles is 5 to 10 m. We use profiles that have their shallowest measurement at a depth of 5 m or less. There are 3465 profiles fitting this criterion in the equatorial North Atlantic region (2°–12°N, 15°–45°W) that we focus on in this study.

For all datasets except Argo, anomalies are calculated with respect to the daily mean seasonal cycle computed using data from 2003–08, when all products are available. Anomalies of Argo-based quantities are calculated based on the 2005–08 monthly mean seasonal cycle. Because of the exceptional strength of the negative AMM event in 2009, our results are not sensitive to the time period used to calculate the seasonal cycles.

### b. PIRATA

Measurements from two PIRATA moorings complement the satellite and reanalysis products. The moorings are located at 4°N, 23°W and 12°N, 23°W (Fig. 2c). Both

moorings measure subsurface temperature, salinity, and velocity, as well as air temperature, relative humidity, wind velocity, rainfall, and shortwave radiation. The mooring at 12°N, 23°W additionally measures downward longwave radiation and barometric pressure. Because of significant gaps in the buoy 10-m velocity records, these data are used only for validation of OSCAR currents and are not used directly in the temperature budget analyses.

Subsurface temperature at 12°N, 23°W is measured at depths of 1, 5, 10, and 13 m, and with 20-m spacing between 20 and 140 m. Measurements are made at the same depths at the 4°N, 23°W mooring except that data at 5 m are not available. Salinity is available from both moorings at depths of 1, 10, 20, 40, 60, and 120 m. In addition, the mooring at 12°N measures salinity at 5 and 80 m. Missing data in the temperature records are filled with vertical linear interpolation. At 12°N, 23°W temperature is missing at depths of 13 and 20 m during 2008. At 4°N, 23°W temperature is missing at 10 m in 2007. Gaps in the salinity records occur at 5 and 20 m during 2008 at the 12°N location and at 10 m during 2007 at the 4°N mooring.

## 3. Methodology

In this section the methods used to analyze the causes of the 2009 AMM event are presented. We first describe how Ekman pumping is calculated from satellite winds. We then present the methodology used to assess the mixed layer temperature balance in the North Atlantic (2°N–25°N), first from satellite, reanalysis, and Argo data and then using measurements from two PIRATA moorings.

### a. Ekman pumping

To calculate Ekman pumping velocity, we first follow Cane (1979) and Lagerloef et al. (1999) and assume a steady linear momentum balance in the upper ocean:

$$-fh_e v_e = \frac{\tau^x}{\rho} - ru_e, \quad (1)$$

$$fh_e u_e = \frac{\tau^y}{\rho} - rv_e. \quad (2)$$

Here  $h_e$  is a constant depth of 30 m and  $r$  is a frictional damping coefficient set to  $2 \times 10^{-4}$  m s<sup>-1</sup>. The values of  $h_e$  and  $r$  were determined empirically from the motion of surface drifting buoys in the global equatorial ocean (Lagerloef et al. 1999). Ekman pumping velocity is then calculated from (1) and (2) as the divergence of the Ekman transport:

$$\begin{aligned}
w_e &= h_e \nabla \cdot \mathbf{v}_e \\
&= \frac{-2rh_e^3 f \beta \tau^y}{\rho(r^2 + h_e^2 f^2)^2} + \frac{h_e^2 f \frac{\partial \tau^y}{\partial x} + rh_e \frac{\partial \tau^y}{\partial y}}{\rho(r^2 + h_e^2 f^2)} \\
&\quad + \frac{2h_e^3 f^2 \beta \tau^x}{\rho(r^2 + h_e^2 f^2)^2} + \frac{-h_e^2 f \frac{\partial \tau^x}{\partial y} + rh_e \frac{\partial \tau^x}{\partial x} - h_e^2 \beta \tau^x}{\rho(r^2 + h_e^2 f^2)}. \tag{3}
\end{aligned}$$

### b. Mixed layer temperature balance

This section presents the details of the mixed layer temperature balance used to determine the processes responsible for the anomalous events in 2009. The methodology used to assess the basin-scale temperature balance in the tropical North Atlantic is described first. We then describe the methodology used to quantify the temperature balance at two PIRATA mooring locations.

#### 1) TROPICAL NORTH ATLANTIC

The mixed layer temperature balance at a given location in the tropical North Atlantic can be written

$$\frac{\partial T'}{\partial t} = \frac{Q'_0}{\rho c_p h} - \frac{\overline{Q_0} h'}{\rho c_p h^2} - (\mathbf{v} \cdot \nabla T)' + \left( \frac{\partial T}{\partial t} \right)_z'. \tag{4}$$

Here overbars indicate the mean seasonal cycle and primes indicate anomalies from the monthly mean seasonal cycle. The term on the left is the change in mixed layer temperature. The terms on the right-hand side are the changes in mixed layer temperature due to anomalies of the surface heat flux ( $Q_0$ ), anomalies of mixed layer thickness acting on the mean surface heat flux, horizontal temperature advection, and the vertical heat flux at the base of the mixed layer. The second term on the right arises from a perturbation expansion of the surface heat flux term around  $h$  assuming  $h' < \bar{h}$ . Also,  $T$  is vertically averaged temperature in the mixed layer,  $h$  is the mixed layer thickness, and  $\mathbf{v}$  is horizontal velocity averaged vertically in the mixed layer.

The temperature tendency due to the vertical heat flux at the base of the mixed layer can be written

$$\left( \frac{\partial T}{\partial t} \right)_z' = - \left( \frac{H \Delta T w_{\text{entr}}}{h} \right)' - \left( \frac{K_v}{h} \frac{\partial T}{\partial z} \right)'. \tag{5}$$

The first term on the right is the mixed layer temperature change due to entrainment. Here  $H$  is the Heaviside unit function ( $H = 0$  if  $w_{\text{entr}} < 0$  and  $H = 1$  otherwise),  $\Delta T$  is the temperature jump at the base of the mixed

layer, and  $w_{\text{entr}}$  is entrainment velocity. Entrainment velocity is defined following McPhaden (1982):

$$w_{\text{entr}} = \frac{\partial h}{\partial t} - \frac{\partial Z_{20}}{\partial t}. \tag{6}$$

In (6),  $h$  is the mixed layer thickness and  $Z_{20}$  is the depth of the 20°C isotherm, defined as positive downward. Positive entrainment, which tends to cool the mixed layer, will occur when  $w_{\text{entr}}$  is positive (e.g., when the mixed layer deepens faster than the thermocline or shoals more slowly).

We parameterize the temperature jump at the base of the mixed layer in the entrainment term as  $\Delta T = T - T_{h|10}$ , where  $T_{h|10}$  is the temperature 10 m below the base of the mixed layer. This parameterization gives  $\Delta T = 1.5^\circ\text{C}$  averaged over 2°–25°N, 15°–45°W during January–April (JFMA), which is consistent with  $\Delta T$  used in previous studies (e.g., Hayes et al. 1991; Foltz et al. 2010). In reality,  $\Delta T$  likely depends on a number of factors, such as stratification below the mixed layer and the magnitude of  $w_e$ . We therefore anticipate a relatively high degree of uncertainty in our estimates of entrainment.

The second term on the right-hand side of (5) is the mixed layer temperature change due to vertical turbulent diffusion. Here  $K_v$  is the eddy diffusion coefficient and  $\partial T / \partial z$  is the average vertical temperature gradient between the base of the mixed layer and 10 m below the mixed layer. The  $K_v$  parameter is difficult to quantify. Hayes et al. (1991) estimated  $K_v = (0.3 - 2.3) \times 10^{-4} \text{ m}^2 \text{ s}^{-1}$  at 0°, 110°W in the eastern equatorial Pacific. For simplicity, we use a constant value of  $K_v = 1 \times 10^{-4} \text{ m}^2 \text{ s}^{-1}$ . There are significant uncertainties associated with our assumption of a constant eddy diffusivity in (5). We therefore expect a high degree of uncertainty in our estimates of turbulent diffusion.

We calculate  $T$  from monthly averaged TMI–AMSR-E SST. Individual Argo temperature and salinity profiles during 2005–09 are used to calculate monthly averaged  $h$ ,  $\Delta T$ , and  $Z_{20}$ . The mixed layer depth is calculated using the criterion of the density equivalent of a 0.3°C decrease from a depth of 5 m. Results are similar for criteria ranging from 0.2° to 0.5°C. The net surface heat flux consists of the latent, sensible, shortwave, and longwave heat fluxes. The shortwave and longwave components are obtained from the TropFlux analysis. We calculate the amount of SWR penetrating through the base of the mixed layer as  $Q_{\text{pen}} = 0.47 Q_{\text{sfc}} e^{-h/15}$ , where  $Q_{\text{sfc}}$  is the net surface SWR assuming an albedo of 6%. The longwave and sensible heat fluxes are generally weak compared to the latent and shortwave components. Anomalies of horizontal temperature advection are calculated from satellite-derived OSCAR currents and

satellite SST gradients calculated over a centered distance of  $2^\circ$ .

Each of the terms in (6) is calculated at a  $1^\circ$  spatial resolution in the tropical Atlantic ( $10^\circ\text{S}$ – $30^\circ\text{N}$ ,  $10^\circ\text{E}$ – $60^\circ\text{W}$ ). To quantify the temperature balance, the terms in (6) are also area averaged in specific regions. To average the horizontal advection term, we follow Lee et al. (2004) and calculate the anomalous change in mixed layer temperature due to horizontal advection as

$$\left(\frac{\partial T}{\partial t}\right)_{\text{adv}}' = \frac{(u_w \delta T_w)' - (u_e \delta T_e)'}{\Delta x} + \frac{(v_s \delta T_s)' - (v_n \delta T_n)'}{\Delta y}. \quad (7)$$

Here  $u$  and  $v$  are zonal and meridional velocity from OSCAR, respectively,  $\delta T$  is the difference between the tropical Atlantic SST and SST averaged in the region, and  $\Delta x$  and  $\Delta y$  are the distances along the zonal and meridional boundaries of the region, respectively. The subscripts  $w$ ,  $e$ ,  $s$ , and  $n$  represent averages along the western, eastern, southern, and northern boundaries, respectively.

We use the convention that a positive surface heat flux tends to warm the ocean. Error estimates for the anomalous change in  $T$  and the sum of the terms on the right-hand side of (6) are shown in Table 2 and discussed in the appendix.

## 2) PIRATA MOORINGS

The mixed layer temperature balance equation that we apply at the PIRATA mooring locations is similar to that used for the area-averaged analysis [(4)]:

$$\frac{\partial T'}{\partial t} = \left(\frac{Q_0}{\rho c_p h}\right)' + Q'_{\text{ocean}}, \quad (8)$$

$$Q'_{\text{ocean}} = -(\mathbf{v} \cdot \nabla T)' + \left(\frac{\partial T}{\partial z}\right)'_z. \quad (9)$$

Here all terms are as in (4). Terms in (8) are defined as positive when they tend to heat the mixed layer. Mixed layer thickness,  $\Delta T$ ,  $\partial T/\partial z$ ,  $Z_{20}$ , entrainment, latent and sensible heat fluxes, and the penetrative component of SWR are calculated as in section 3c(1) using daily averages of buoy air temperature, relative humidity, wind speed, SWR, and subsurface temperature and salinity. Mixed layer temperature is calculated using buoy subsurface temperature and mixed layer depth. Mixed layer depth is estimated using the criterion of the density equivalent of  $0.3^\circ\text{C}$  temperature decrease from a depth of 1 m.

Horizontal advection [first term on the right in (9)] is calculated from daily OSCAR currents and TMI–AMSR-E

TABLE 2. 2009 anomalies of terms in the mixed layer temperature balance, averaged in the ENA region ( $2^\circ$ – $12^\circ\text{N}$ ,  $15^\circ$ – $45^\circ\text{W}$ ) during (left) JF, (middle) MA, and (right) the total for the JFMA period. The first four rows indicate the anomalous change in mixed layer temperature due to, respectively, latent heat flux, anomalies of absorbed shortwave radiation, anomalies of mixed layer depth acting on the mean surface heat flux; and vertical heat flux at the base of the mixed layer. The fifth row is the sum of the first four rows, and last row is observed (TMI–AMSR-E) anomalous change in SST. Units are  $^\circ\text{C}$ . Errors for the sum and observed values are one standard error.

	Jan–Feb	Mar–Apr	Total
LHF	-0.3	0.7	0.4
SWR	0.2	0.5	0.7
MLD	0.0	-0.2	-0.2
Vertical	-1.2	-1.1	-2.3
Sum	$-1.3 \pm 0.5$	$-0.1 \pm 0.5$	$-1.4 \pm 0.7$
Observed	$-0.9 \pm 0.1$	$-0.2 \pm 0.1$	$-1.1 \pm 0.2$

SST. The OSCAR zonal currents agree reasonably well with zonal currents at a depth of 10 m from the moorings. The meridional currents are more poorly represented by OSCAR. The correlation between 5-day averaged buoy and OSCAR zonal velocity at  $12^\circ\text{N}$ ,  $23^\circ\text{W}$  is 0.7, based on  $\sim 2$  yr of daily data. The record-length mean is  $-6.7 \text{ cm s}^{-1}$  for OSCAR and  $-3.8 \text{ cm s}^{-1}$  for the mooring. For the meridional component the correlation is 0.4, and the mean of the mooring velocity is  $2.0 \text{ cm s}^{-1}$ , while for OSCAR the mean is  $-0.1 \text{ cm s}^{-1}$ . At  $4^\circ\text{N}$ ,  $23^\circ\text{W}$  the correlation for the zonal component is 0.8, and for the meridional component the correlation is zero. The record-length means for the zonal component are  $8.3 \text{ cm s}^{-1}$  for the mooring and  $6.3 \text{ cm s}^{-1}$  for OSCAR at this location. For the meridional component the means are  $3.3 \text{ cm s}^{-1}$  for the mooring and  $0 \text{ cm s}^{-1}$  for OSCAR. These uncertainties in OSCAR currents translate to errors in the temperature balance of  $\pm 0.1^\circ$ – $0.2^\circ\text{C month}^{-1}$  (see the appendix).

We use daily TropFlux net longwave radiation at  $4^\circ\text{N}$ ,  $23^\circ\text{W}$  and calculate net longwave emission at  $12^\circ\text{N}$ ,  $23^\circ\text{W}$  using direct measurements of downward LWR at the mooring. Because of gaps in the buoy time series, anomalies for the November 2008–November 2009 period are calculated with respect to either the same period during 2007–08 (at  $12^\circ\text{N}$ ,  $23^\circ\text{W}$ ) or 2006–07 ( $4^\circ\text{N}$ ,  $23^\circ\text{W}$ ). Error estimates for each term in (8) and (9) are discussed in the appendix, and error bars for  $Q_{\text{ocean}}$  and horizontal advection (the terms with the largest errors) are shown later (see Figs. 6 and 7).

## 4. Results

In this section we examine the processes responsible for generating the SST anomalies in the North Atlantic

( $2^{\circ}$ – $25^{\circ}$ N,  $15^{\circ}$ – $45^{\circ}$ W) during 2009. A description of the surface conditions is presented first, followed by an analysis of the mixed layer temperature budget.

#### a. Evolution of the 2009 anomalies

The SST anomalies in 2009 developed over a span of several months and were strongest between  $10^{\circ}$ S and  $25^{\circ}$ N (Fig. 2). In January 2009 there was an anomalous intensification of the northeasterly trade winds in the tropical North Atlantic (TNA:  $12^{\circ}$ – $25^{\circ}$ N) coincident with anomalously cold SSTs centered near  $20^{\circ}$ N and warmer than normal SSTs in the tropical South Atlantic (Fig. 2a). Surface wind speed anomalies during January peaked at  $\sim 2 \text{ m s}^{-1}$  in the  $15^{\circ}$ – $20^{\circ}$ N band, decreasing to  $0.5$ – $1 \text{ m s}^{-1}$  just north of the equator. Cold SST anomalies were strongest in the northeastern basin, reaching a maximum of  $1^{\circ}$ – $1.5^{\circ}$ C off the coast of northwest Africa (Fig. 2a). To the south of the strongest anomalous cooling, a band of weaker negative SST anomalies developed between the equator and  $5^{\circ}$ N. This band of anomalously cold SSTs was associated with anomalous northerly winds between  $20^{\circ}$  and  $40^{\circ}$ W centered near  $\sim 2^{\circ}$ N (Fig. 2a). The sign of the meridional wind and SST gradient anomalies in this region is consistent with forcing of the northerly wind anomalies by the southward anomalous SST gradient (e.g., Lindzen and Nigam 1987).

By March 2009 the anomalously strong trade winds had relaxed in the TNA, with anomalously low wind speed between  $10^{\circ}$  and  $20^{\circ}$ N (Fig. 2b). The strongest negative SST anomalies in March were located farther south, between the equator and  $15^{\circ}$ N, increasing in magnitude northeastward from the coast of Brazil to a maximum of  $3^{\circ}$ C off the coast of northwest Africa. Anomalous northerly winds on the southern edge of the band of coldest SST anomalies ( $5^{\circ}$ S– $2^{\circ}$ N) intensified between January and March (Figs. 2a,b). The southward progression of the strongest SST and wind anomalies during boreal winter and spring is consistent with wind evaporation–SST (WES) feedback (Xie 1999; Chang et al. 2001) and the canonical AMM presented in Chiang et al. (2002).

Between March and May the region of strongest cold SST anomalies off the coast of northwest Africa weakened slightly and shifted southwestward (Fig. 2c). Northerly surface wind anomalies between  $2^{\circ}$ N and  $5^{\circ}$ S strengthened further, especially in the western basin. SSTs became anomalously warm between  $2^{\circ}$ N and  $5^{\circ}$ S, peaking at  $>1^{\circ}$ C between  $10^{\circ}$  and  $20^{\circ}$ W. The warm SST anomalies in the equatorial South Atlantic were much shorter lived than the cold anomalies to the north, however. By July the warm anomalies on the equator were replaced by cold anomalies of up to  $2^{\circ}$ C (Fig. 2d). Foltz and McPhaden (2010a) showed that the strong equatorial cooling was caused by the western boundary reflection of

upwelling Rossby waves, generated by northwesterly wind stress anomalies the previous spring, into upwelling equatorial Kelvin waves. Between May and July SSTs became anomalously warm to the north of  $15^{\circ}$ N, and the cold SST anomalies between the equator and  $15^{\circ}$ N weakened considerably. Surface winds returned to normal throughout most of the basin.

The initial trigger for the strong meridional mode event in 2009 can be traced to the anomalous intensification of the TNA trade winds in January and February (JF). The enhanced trade winds are consistent with La Niña conditions in the eastern equatorial Pacific during the winter of 2008–09 and a positive NAO index in January 2009 (Table 1). The anomalously strong trade winds in JF 2009 cannot be explained entirely by ENSO and the NAO, however: The 2008 La Niña in the Pacific was stronger than the La Niña in 2009, and the NAO index was of the same sign and comparable in magnitude during the two years (Table 1). Based on the NAO and ENSO indices for 2008 and 2009, therefore, wind speed in the TNA during these years should have been similar. Instead, winds were slightly weaker than normal in JF 2008, but two standard deviations stronger than normal in JF 2009 (Table 1).

The stronger winds in 2009 relative to 2008 can be explained in part by a stronger than normal subtropical Atlantic high pressure system (STH) in 2009 compared to 2008. Changes in the strength of the STH account for part of the NAO variability, along with changes in atmospheric circulation in the subpolar Atlantic (Wallace and Gutzler 1981). It is therefore possible for strong fluctuations in the STH to occur without corresponding fluctuations in the NAO index if the STH and subpolar Atlantic vary in phase. Indeed, the STH was 1.5 standard deviations above normal in January 2009, compared to one standard deviation below normal in January 2008 despite positive values of the NAO index in both years (Table 1). The strong influence of the STH on TNA wind speed during 2008–09, independent of the NAO and ENSO, is consistent with a statistical analysis for 1982–2009. Multiple linear regression using the NAO, Niño-3.4, and STH indices explains 80% of tropical North Atlantic wind speed variance in January, compared to 55% when the predictors are limited to the NAO and Niño-3.4 indices. The persistence of strong positive wind speed anomalies from JF 2009 despite a negative NAO index and weakly positive STH may be due to stronger than normal convection in the Amazon during February 2009 (Table 1), consistent with Enfield and Mayer (1997) and Saravanan and Chang (2000).

The development of cold SST anomalies in the TNA in January coincident with stronger than normal trade winds suggests that the SST anomalies here were forced

primarily by enhanced wind-induced evaporative heat loss, consistent with previous studies (Cayan 1992; Carton et al. 1996; Tanimoto and Xie 2002; Foltz and McPhaden 2006). Following the initial cooling in the TNA in January 2009, cold SST anomalies persisted between  $2^{\circ}$  and  $12^{\circ}\text{N}$  during February–May 2009 despite much weaker wind speed anomalies in this region (Figs. 2b,c). This is the time of year when positive WES feedback is strongest in the western tropical Atlantic (Xie and Carton 2004). It is therefore possible that WES feedback contributed to the strong anomalous cooling in the equatorial North Atlantic (ENA:  $2^{\circ}$ – $12^{\circ}\text{N}$ ,  $15^{\circ}$ – $45^{\circ}\text{W}$ ) and rapid development of the AMM during February–May 2009. In the next two sections we analyze the processes responsible for the generation and persistence of the cold SST anomalies in the ENA during JFMA 2009.

#### b. Ekman pumping and vertical turbulent fluxes

Previous studies suggest that on interannual time scales SST anomalies in the TNA are driven primarily by changes in wind-induced latent heat flux (LHF). In contrast, in the equatorial Atlantic ( $12^{\circ}\text{S}$ – $12^{\circ}\text{N}$ ) surface heat fluxes appear to be less important relative to ocean dynamics, especially in the central and eastern basin (Carton and Huang 1994; Carton et al. 1996; Foltz and McPhaden 2006). Therefore, we expect that ocean dynamics may have contributed significantly to the development of the cold SST anomalies in this ENA region during January–May 2009. One candidate is anomalous Ekman pumping, driven by anomalous northwesterly winds in the equatorial Atlantic (Fig. 2). Foltz and McPhaden (2010a) showed that the anomalous northwesterlies in early 2009 generated upwelling equatorial Rossby waves, which, in addition to Ekman pumping, may have contributed to anomalous cooling of SST. In this section we first focus on the role of Ekman pumping, a mechanism that was not considered by Foltz and McPhaden (2010a). We then discuss entrainment and vertical turbulent diffusion, which implicitly include the contributions from equatorial waves and Ekman dynamics.

In most of the tropical Atlantic, poleward of  $10^{\circ}$  and away from the African coast, climatological Ekman pumping is weak and negative (i.e., downwelling) during JFMA (Fig. 3a). Positive Ekman pumping (i.e., upwelling) of less than  $0.3 \text{ m day}^{-1}$  is present in the eastern basin poleward of  $5^{\circ}$ . There is a narrow band of stronger Ekman pumping ( $>1 \text{ m day}^{-1}$ ) centered just south of the equator and a band of strong negative values just north of the equator in the eastern basin, consistent with Chang and Philander (1994).

During boreal winter and spring 2009 there was Ekman pumping of  $\sim(0.3\text{--}1.5) \text{ m day}^{-1}$  between the equator and

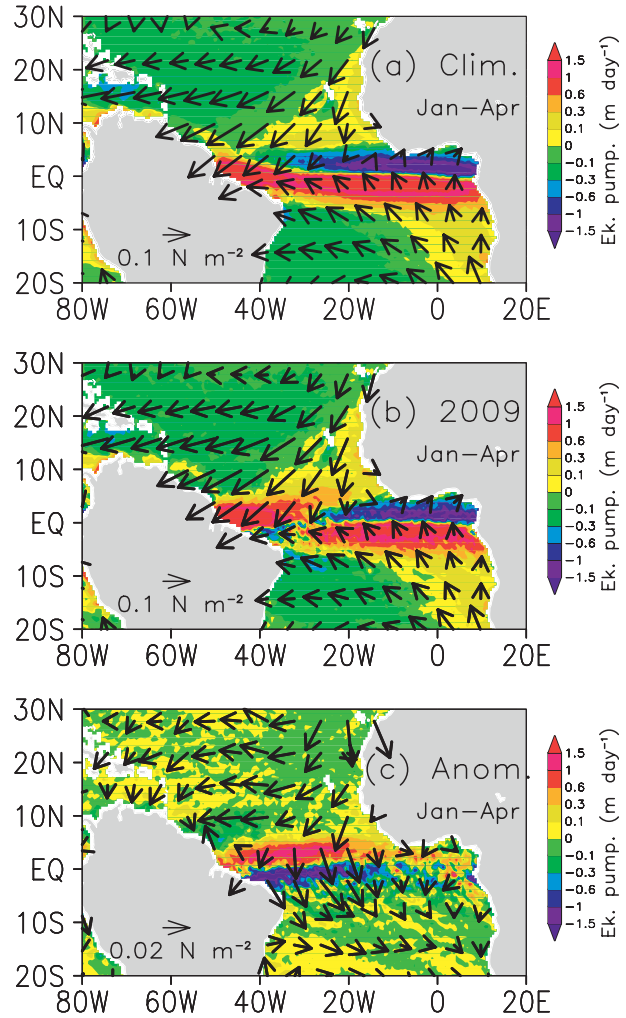


FIG. 3. The (a) 2003–08 climatologies of Ekman pumping velocity (shaded,  $>0$  indicates upwelling) and wind stress (vectors) during January–April (JFMA). (b) JFMA 2009 Ekman pumping velocity and wind stress. (c) JFMA 2009 anomalies of Ekman pumping velocity and wind stress with respect to 2003–08 climatologies.

$6^{\circ}\text{N}$ , west of  $20^{\circ}\text{W}$ , in a region where there is normally negative Ekman pumping (i.e., downwelling) or very weak upwelling (Fig. 3b). Ekman pumping anomalies in JFMA 2009 reached  $1 \text{ m day}^{-1}$  in a narrow band centered near  $3^{\circ}\text{N}$  between  $20^{\circ}$  and  $40^{\circ}\text{W}$ . Anomalous Ekman pumping here was driven primarily by the meridional component of wind stress (Fig. 3c). Anomalous northerly wind stress acting on the meridional gradient of planetary vorticity [the beta effect; first term on the right in (3)], combined with the westward increase in anomalous northerly wind stress [the curl effect; second term on the right in (3)] and anomalous meridional wind stress divergence [third term on the right in (3)], all contributed to positive Ekman pumping anomalies between the

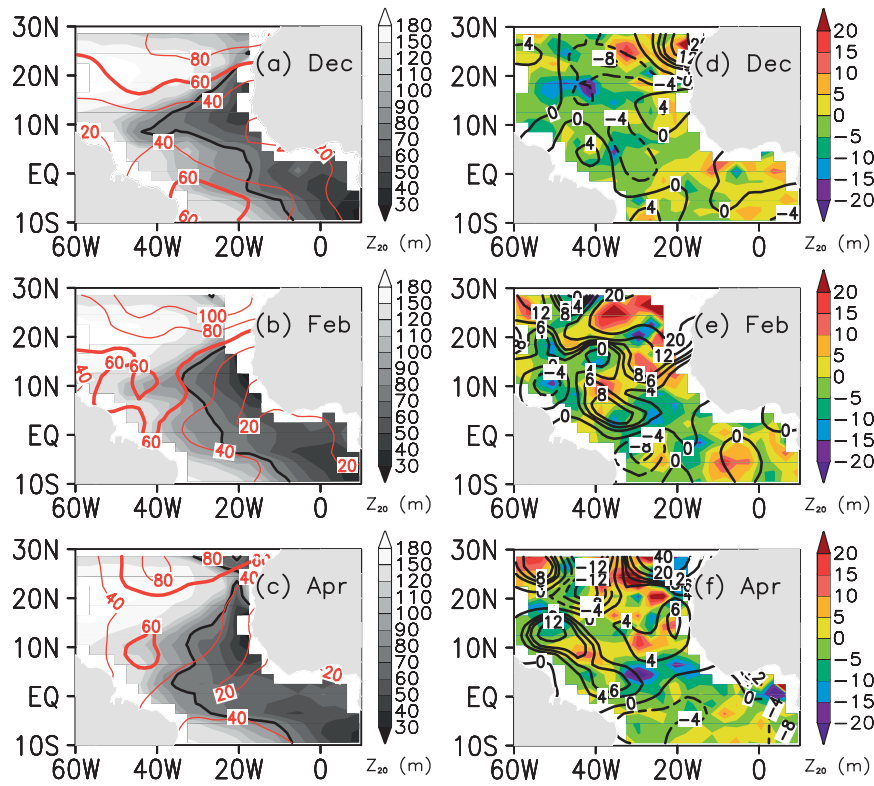


FIG. 4. (left) Climatological (2003–08) mixed layer depth (red contours, with 60 m highlighted in bold) and depth of the 20°C isotherm (shading, with 80 m contoured in black) during (a) December, (b) February, and (c) April. (right) As at left, but contours are 2009 anomalies (with respect to 2005–08) of MLD, and shading represents 2009 anomalies of  $Z_{20}$ .

equator and 6°N. The strongest Ekman pumping anomalies coincided with anomalous shoaling of the thermocline of  $\sim 10$  m (Figs. 4d–f).

During January and February, there was also pronounced anomalous deepening of the mixed layer between the equator and 30°N (Figs. 4d–f), which was most likely driven by enhanced turbulent mixing associated with the anomalously strong trade winds during the same period (Figs. 2a and 3c). The anomalous mixed layer deepening was strongest to the north of the strongest Ekman pumping and thermocline depth anomalies, where the wind speed anomalies were greatest.

The anomalous Ekman pumping and mixed layer deepening would have tended to cool SST anomalously through the combination of entrainment and vertical turbulent diffusion. The climatological entrainment velocity is positive between the equator and 10°N during JF, when the mixed layer is deepening to the west of 30°W, and  $Z_{20}$  is shoaling in the east (Figs. 4a–c). The strongest anomalous entrainment velocity in 2009 also occurs in this region and during JF, the period with anomalous mixed layer deepening and anomalous shoaling of the thermocline (Figs. 4d–f). Anomalous cooling

from turbulent diffusion is likely to be strongest during March and April (MA) in the eastern basin ( $2^{\circ}$ –10°N, 15°–30°W), since this is where anomalous shoaling of the thermocline is most pronounced (Fig. 4f). A shallower than normal thermocline will tend to increase the vertical temperature gradient below the mixed layer, enhancing cooling from turbulent mixing according to (5). The results of this qualitative analysis are generally consistent with the location and timing of the strongest anomalous cooling of SST in the tropical North Atlantic during 2009 (Fig. 5a).

### c. Mixed layer temperature balance

To quantify the contributions from the vertical and surface heat fluxes to the anomalous cooling in early 2009, we consider the mixed layer temperature budget (4). During JF 2009, anomalous cooling of SST was strongest between the equator and  $\sim 15^{\circ}$ N (Fig. 5a). The cooling was driven primarily by stronger than normal latent heat flux and net vertical heat flux (Figs. 5b–e). In MA, there was additional anomalous cooling in the  $2^{\circ}$ –12°N band and anomalous warming to the north and south (Fig. 5f). Anomalies of LHF and  $h' \overline{Q}_0$  contributed to the

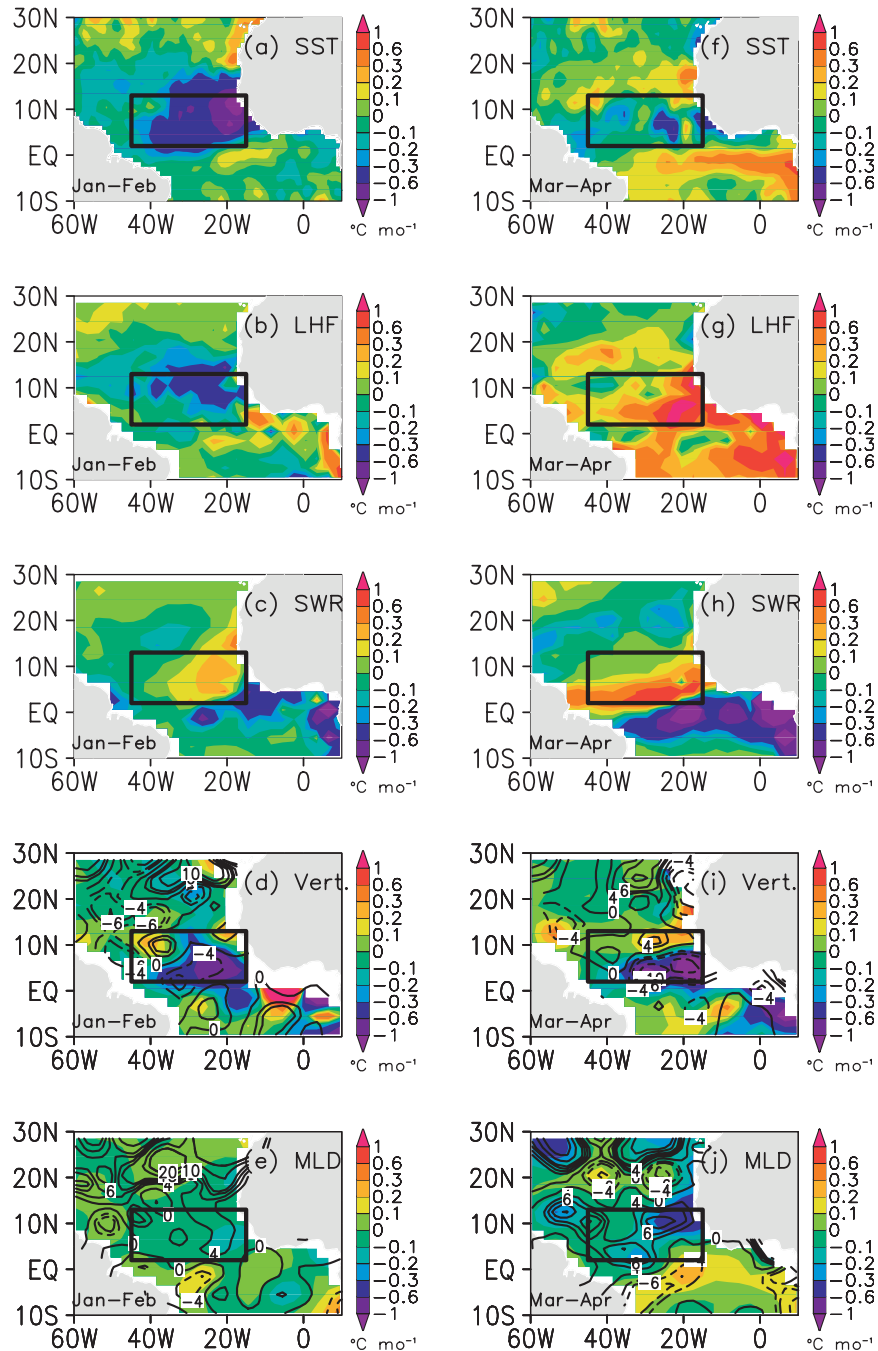


FIG. 5. Terms in the mixed layer temperature budget [(4)] averaged during (left) January–February (JF) 2009 and (right) March–April (MA) 2009. Negative values indicate anomalous cooling of SST. (a),(f) Rate of change of SST. (b),(g) LHF. (c),(h) Surface SWR. (d),(i) Vertical heat flux at the base of the mixed layer, with contours shown for anomalies of 20°C isotherm depth (positive values for deeper than normal and negative values for shallower than normal). (e),(j) Mixed layer depth (MLD) anomalies acting on the mean surface heat flux, with contours shown for MLD anomalies (positive for deeper than normal and negative for shallower than normal).

anomalous warming outside of the 2°–12°N band during MA (Figs. 5g,j). Between 2° and 12°N, anomalous cooling from the net vertical heat flux and  $h'\overline{Q}_0$  was balanced by strong anomalous warming from LHF and shortwave radiation (SWR). Horizontal temperature advection tended to cool the mixed layer anomalously in the eastern basin between 5° and 15°N, where westward mean currents and anomalous zonal SST gradients were strongest. Averaged between 2° and 25°N, however, its contribution to the anomalous cooling was small compared to surface fluxes and the net vertical heat flux.

We next focus on the equatorial North Atlantic region (2°–12°N, 15°–45°W) for a quantitative assessment of the mixed layer temperature balance. Our selection of this region is based on several factors. First, the SST anomalies in this region were generally much stronger than those to the north and south. The processes responsible for generating the SST anomalies in this region are therefore more likely to be resolved above observational noise and uncertainties associated with uneven sampling. Second, based on our qualitative analysis, the temperature budget in the ENA region appears to be a balance among several terms, including vertical heat fluxes, LHF, SWR, and  $h'\overline{Q}_0$ . Quantifying these terms in relation to anomalous changes in SST will help to determine which processes are most important. Finally, the ENA region is sampled by a larger number of Argo floats compared to the equatorial band, and there are two PIRATA moorings in the ENA region that were well positioned to record the strong anomalies in early 2009 (Fig. 2; see also section 5). Because of strong spatial variability of the temperature budget in the ENA (Fig. 5), we calculate the terms in (6) averaged in four subregions [northeast (NE): 7°–12°N, 15°–30°W; northwest (NW): 7°–12°N, 30°–45°W; southwest (SW): 2°–7°N, 30°–45°W; and southeast (SE): 2°–7°N, 15°–30°W] and then average each of the subregions to obtain the temperature balance in the ENA region as a whole.

During JF both wind-induced LHF and the net vertical heat flux contributed significantly to the observed cooling in the ENA region (Table 2). Anomalous cooling from the vertical heat flux was 4 times as strong as the cooling from wind-induced LHF. Entrainment and turbulent diffusion contributed equally to the anomalous cooling from vertical processes. Entrainment was driven by anomalous mixed layer deepening in the NW, NE, and SW subregions, and thermocline shoaling in the SE subregion. Anomalies of turbulent diffusion were driven by anomalous shoaling of the thermocline, and associated increase in  $\partial T/\partial z$ , in the SE subregion. As a result, the strongest anomalies of the net vertical heat flux were concentrated in the eastern basin (NE and SE subregions; Fig. 5d), where anomalous entrainment and

turbulent diffusion were strongest and where there is a shallow mean mixed layer and thermocline (Fig. 4b). Anomalous cooling from wind-induced LHF was strongest in the NE subregion (Fig. 5b), where the wind speed anomaly was strongest and the climatological mixed layer is thinnest. The good agreement between the sum of LHF, SWR, and vertical heat flux with the observed change of SST in the ENA region suggests that other processes, such as horizontal temperature advection, were relatively unimportant, or that they canceled one another (Table 2).

After the initial anomalous cooling of 1°C in JF, subsequent cooling during MA was relatively weak. The weaker cooling during MA is a consequence of an anomalous warming tendency of 0.7°C due to LHF-induced damping of the anomalously cold SST driven by the anomalous air-sea humidity difference, combined with a warming tendency of 0.5°C from the enhanced SWR associated with the southward anomalous displacement of the ITCZ (Figs. 5f–h; Table 2). The surface flux-induced anomalous warming is balanced to within 0.1°C by the cooling tendency from the combination of the net vertical heat flux and anomalous cooling from the dilution of the mean positive surface heat flux over a thicker mixed layer (i.e., a reduction in the ability of the surface flux to warm SST due to the increased volume of the mixed layer) (Figs. 5i,j). The anomalous cooling from vertical processes was dominated by turbulent diffusion, which itself was driven by anomalous shoaling of the thermocline in the SE subregion.

In summary, the anomalous cooling in the equatorial North Atlantic (2°–12°N) during JF 2009 was driven by a combination of enhanced wind-induced latent heat loss and the vertical heat flux at the base of the mixed layer. After the initial cooling, SSTs remained anomalously cold during MA because of a balance between the combination of the vertical heat flux and dilution of the surface heat flux over a thicker mixed layer, tending to cool the mixed layer anomalously, and the combination of anomalous warming from enhanced SWR due to the anomalous southward shift of the ITCZ, and air-sea humidity-induced evaporation, tending to damp the cold anomaly back to climatology.

## 5. PIRATA mooring locations

In this section we analyze the mixed layer temperature balance (8) at two PIRATA mooring locations in the ENA region (12°N, 23°W and 4°N, 23°W) (Figs. 2c,d). The advantages of using measurements from the moorings are the increased temporal resolution of subsurface temperature and salinity measurements (daily from the moorings versus monthly from Argo) and more accurate

measurements of surface fluxes from the moorings compared to satellites and atmospheric reanalyses. The temperature budgets at the mooring locations therefore complement the area-averaged analysis presented in the previous section.

#### a. 12°N, 23°W

The PIRATA mooring at 12°N, 23°W was located to the northwest of the strongest cold SST anomalies in March–May 2009 (Figs. 2b,c). There was strong anomalous cooling at this location during JF 2009, consistent with satellite SSTs during the same period (Fig. 6a). The anomalous cooling at the mooring location corresponds to a period with stronger than normal wind speed and a pronounced anomalous deepening of the mixed layer (Fig. 6b). The timing and magnitude of the anomalous mixed layer deepening and wind speed anomalies are consistent with satellite and Argo measurements in the ENA region (Figs. 2 and 4).

Enhanced wind speed in JF at 12°N, 23°W tended to cool the mixed layer anomalously through enhanced LHF. However, when anomalies in mixed layer depth are taken into account, the net impact of LHF on SST during JFMA was anomalous warming due to the dilution of the climatological latent heat loss over a thicker mixed layer (Fig. 6c). The same mechanism played an important role in determining the sign of the SWR-induced SST tendency. There was anomalously strong SWR during mid-January through April 2009, tending to warm the mixed layer anomalously. Dilution of the climatological SWR flux over a thicker mixed layer, however, resulted in a net anomalous cooling tendency due to SWR during JFMA (Fig. 6c). Overall, there was anomalous mixed layer cooling of 1°C between March and April 2009 associated with the dilution of the mean positive surface heat flux over the anomalously thick mixed layer (Fig. 6d). The anomalous cooling associated with the thicker mixed layer is consistent with the cooling observed in the ENA region during the same period (Table 2), although the cooling at the mooring location is significantly stronger. The stronger cooling at the mooring location compared to the ENA region is likely due to the combination of a larger positive climatological net surface heat flux and stronger anomalous mixed layer deepening at the mooring location.

The net surface heat flux agrees reasonably well with the rate of change of mixed layer temperature during late 2008 and early 2009 at 12°N, 23°W (Fig. 6d), although there was stronger anomalous cooling during JF 2009 than predicted by the surface heat flux (Figs. 6d,e). The mismatch can be explained by an anomalous cooling tendency from zonal temperature advection associated with an anomalously strong negative zonal SST gradient

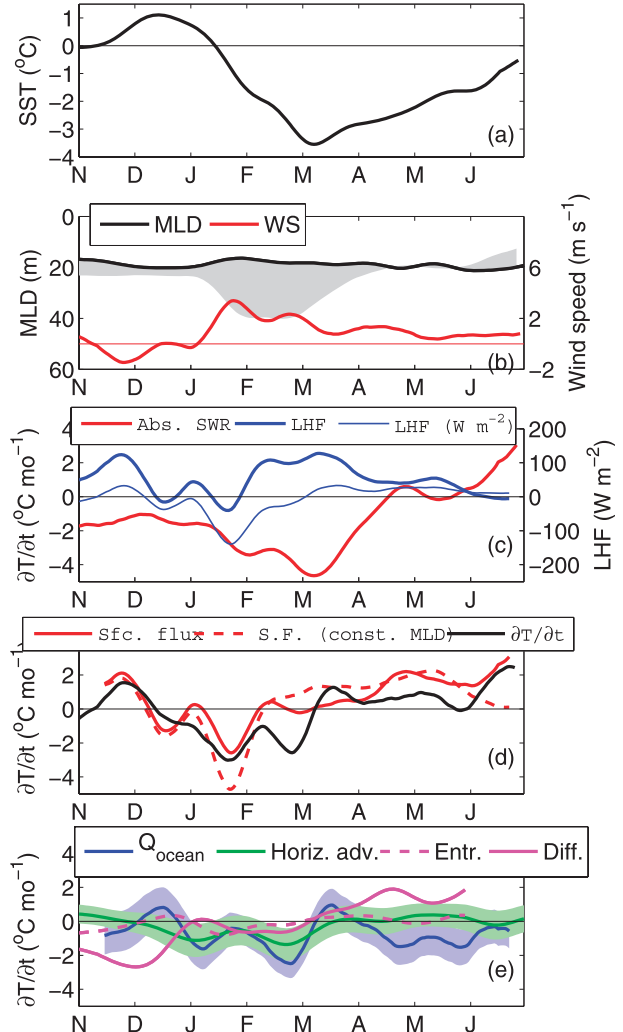


FIG. 6. Measurements from the PIRATA mooring at 12°N, 23°W during November 2008–June 2009 (position of mooring is shown in Fig. 2). (a) SST anomaly. (b) MLD climatology (black) and 2008–09 anomaly (shading), and wind speed anomaly (red). (c) Anomalous contributions from surface LHF (blue) and SWR absorbed in the mixed layer (red) to changes in SST. Thin blue line is the surface LHF. (d) Anomalies of net surface heat flux (solid red), surface heat flux with MLD held constant (dashed red), and mixed layer temperature rate of change (black). (e) Anomalies of the sum of ocean processes (estimated from the residual in the temperature balance and shown as solid blue curve), horizontal temperature advection (green), vertical turbulent diffusion (pink), and entrainment (dashed pink). Blue and green shading represents one standard error. Anomalies are with respect to November 2007–June 2008. Data have been smoothed with a 20-day low-pass filter.

(i.e., strongest anomalous cooling located to the east of the mooring) in combination with climatological westward near-surface currents. The net vertical heat flux was weak at this location during JFMA 2009, consistent with weak climatological downwelling and a deeper

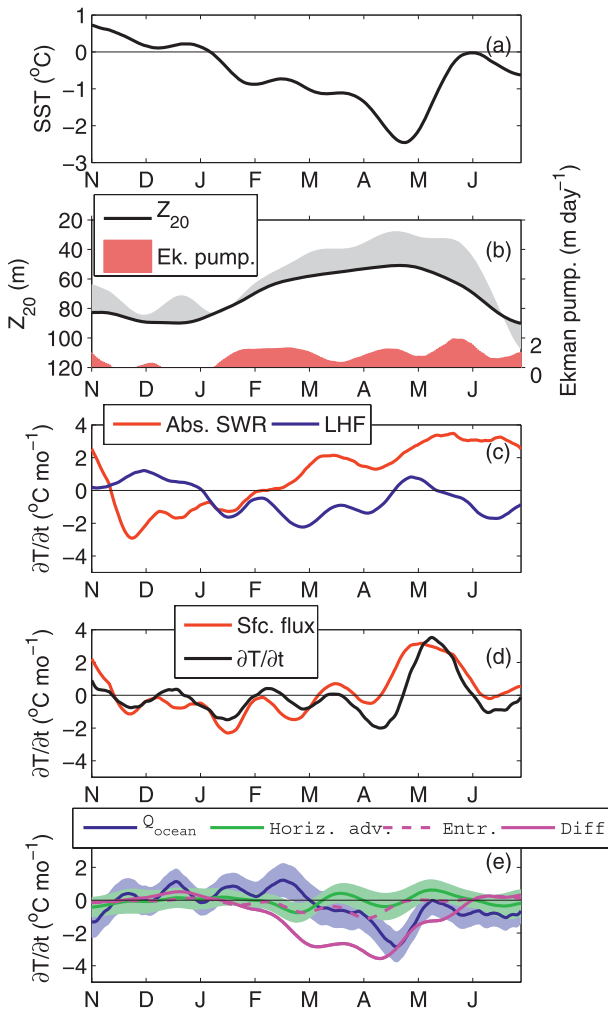


FIG. 7. As in Fig. 6, but from the PIRATA mooring at 4°N, 23°W (location shown in Fig. 2) and anomalies are with respect to November 2006–June 2007. In (b), the black curve is the climatological 20°C isotherm depth ( $Z_{20}$ ), gray shading is the  $Z_{20}$  anomaly, and red shading is Ekman pumping anomaly (positive values indicate upwelling).

than normal thermocline. The small contribution from the vertical heat flux at 12°N, 23°W is consistent with the large-scale analysis presented in the previous section (Figs. 5d,i).

#### b. 4°N, 23°W

The PIRATA mooring at 4°N, 23°W is located in the southeastern corner of the ENA region, where there was strong anomalous cooling and anomalous Ekman pumping during January–March 2009 (Figs. 3c, 4, and 5). The maximum negative SST anomaly occurred in late April at this location, almost two months after the strongest cold anomaly at 12°N, 23°W (Fig. 7a). Anomalous Ekman pumping led to anomalous shoaling of the thermocline

of ~30 m between January and mid-May at 4°N, 23°W (Fig. 7b). This timing is consistent with that found in the ENA region (Fig. 4). The largest thermocline depth anomalies at 4°N, 23°W coincided with the period when the thermocline is shallowest climatologically at this location.

Stronger than normal wind speed during January–March 2009 at 4°N, 23°W tended to cool the mixed layer anomalously through enhanced latent heat loss (Fig. 7c), consistent with the area-averaged temperature budget in the ENA region (Table 2). Anomalous cooling from latent heat loss during February–May 2009 was balanced by a strong anomalous warming tendency associated with positive anomalies of SWR (Fig. 7c). The enhanced SWR at the mooring location during February–June is consistent with the large-scale analysis of the previous section (Figs. 5c,h) and the pronounced anomalous southward shift of the ITCZ during April–May 2009 (Fig. 1b).

The net surface heat flux agrees reasonably well with the mixed layer temperature tendency during late 2008 and early 2009, though there is a period in April with strong anomalous cooling (~2°C month⁻¹) that cannot be explained by the surface heat flux (Figs. 7d,e). April is also the month with the strongest observed anomalous cooling, strong Ekman pumping anomalies, shallower than normal thermocline, and the climatological minimum in thermocline depth. It is therefore anticipated that entrainment and vertical turbulent diffusion were important at the mooring location in April. Indeed, estimates from the mooring data show a broad peak of anomalous cooling from the vertical heat flux during late February through April (Fig. 7e). The presence of strong cooling from the vertical heat flux at 4°N, 23°W is consistent with the analysis based on Argo profiles, which shows a maximum in cooling in the NE and SE subregions (2°–12°N, 15°–30°W) and maximum thermocline shoaling in the SE subregion (2°–7°N, 15°–30°W) (Figs. 4 and 5).

#### 6. Summary and discussion

In January–May 2009 a strong Atlantic meridional mode event developed in the tropical Atlantic. During its peak in boreal spring, there were cold SST anomalies of 0.5°–2°C in the equatorial North Atlantic (2°–12°N) and weaker warm SST anomalies in the equatorial South Atlantic (0°–5°S). In this study the causes of the strong anomalous cooling in the equatorial North Atlantic are analyzed using satellite and in situ datasets.

It is found that the cooling was initiated in January by an anomalous intensification of the subtropical North Atlantic high pressure system and associated increase in

strength of the trade winds in the tropical North Atlantic ( $12^{\circ}$ – $25^{\circ}$ N). Stronger than normal trade winds persisted through February, due in part to a moderate La Niña in the Pacific, a stronger than normal subtropical North Atlantic high pressure system, and anomalously strong convection in the Amazon. Cold SST anomalies formed first near  $20^{\circ}$ N off the coast of Africa, progressed southward to  $2^{\circ}$ – $12^{\circ}$ N, and then intensified and expanded westward during February–May. Surface winds in the equatorial Atlantic responded to the meridional SST gradient, becoming northwesterly in January and intensifying through May, consistent with positive wind evaporation–SST feedback.

The surface wind anomalies forced anomalous Ekman pumping between  $2^{\circ}$  and  $6^{\circ}$ N, shoaling the thermocline anomalously by 10–30 m during January–May. Farther north ( $6^{\circ}$ – $12^{\circ}$ N), stronger than normal trade winds induced anomalous mixed layer deepening of 5–20 m. In each region, the net effect was to bring the thermocline closer to the base of the mixed layer, enhancing cooling from entrainment and vertical turbulent diffusion. The anomalous cooling was partially balanced by positive anomalies of shortwave radiation associated with the pronounced anomalous southward shift of the ITCZ in response to the interhemispheric SST gradient anomaly. Stronger than normal wind-induced evaporative heat loss also contributed significantly to the observed cooling in January and February. Dilution of the positive surface heat flux over an anomalously deep mixed layer (i.e., a reduction in the ability of the surface flux to warm SST due to the increased volume of the mixed layer) tended to cool the mixed layer anomalously during March and April 2009. The mechanisms responsible for generating the SST anomalies in the equatorial North Atlantic during JFMA 2009 are summarized schematically in Fig. 8.

Our results for the event in 2009 are consistent with previous studies, which indicate that surface heat flux anomalies drive most of the interannual and decadal variability of SST in the northern tropical Atlantic, while ocean dynamics play an important role within  $10^{\circ}$  of the equator (Carton et al. 1996; Tanimoto and Xie 2002; Foltz and McPhaden 2006). Our results are also consistent with the modeling study of Chang et al. (2001), which shows that atmospheric internal variability generates SST anomalies in the tropical Atlantic north of about  $15^{\circ}$ N and that coupled feedback is required to generate SST anomalies and cross-equatorial winds in the deep tropics ( $10^{\circ}$ S– $10^{\circ}$ N). In addition, we found a significant enhancement of vertical turbulent cooling in 2009, and we found an anomalous thickening of the mixed layer, which decreased the efficiency with which the net surface heat flux warmed the mixed layer. It is interesting to compare our results to the mechanism

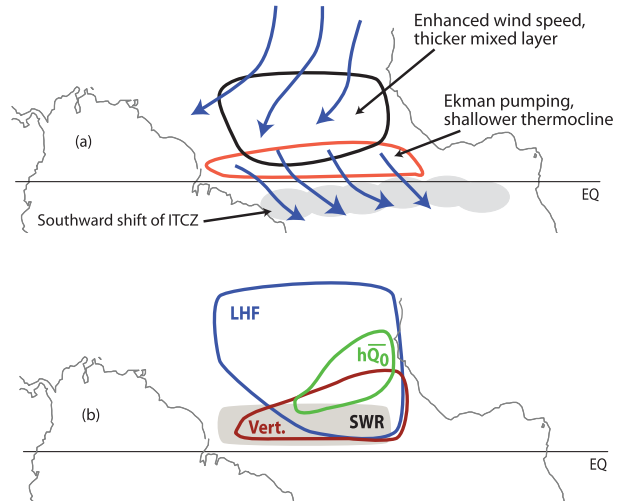


FIG. 8. Schematic diagrams illustrating the processes responsible for generating the SST anomalies during JFMA 2009. (a) Blue arrows represent anomalies of surface wind velocity. (b) Blue region is where anomalies of latent heat flux are important, red is vertical heat flux (entrainment + turbulent diffusion), green is anomalies of mixed layer depth acting on the climatological surface heat flux, and gray shading is surface shortwave radiation.

proposed by Doi et al. (2010). They showed that changes in mixed layer depth in the Guinea Dome region ( $10^{\circ}$ – $15^{\circ}$ N,  $20^{\circ}$ – $35^{\circ}$ W) during boreal fall affect the Atlantic meridional mode the following spring. Anomalous deepening of the mixed layer in the fall dilutes the negative surface heat flux in a thicker layer, tending to increase SST anomalously. In contrast, we find that anomalous deepening of the mixed layer in the spring dilutes the positive surface heat flux, tending to anomalously decrease SST. The opposite effects of changes in MLD on SST during fall and spring result from opposite signs of the net surface heat flux during these seasons.

We found that anomalous cooling from entrainment and vertical turbulent diffusion in the  $2^{\circ}$ – $6^{\circ}$ N band during January–April 2009 was driven in part by strong northwesterly wind anomalies and resultant Ekman pumping. Foltz and McPhaden (2010a,b) showed that the wind stress field associated with a negative meridional mode in the spring (colder than normal SSTs north of the equator relative to the south, as occurred in 2009) generates upwelling equatorial Rossby waves north of the equator. The generation of upwelling Rossby waves is consistent with the observed southwestward propagation of the strongest cold SST anomalies during January–April 2009. Further studies are needed to quantify the contributions from Ekman dynamics and equatorial waves to thermocline depth and SST anomalies in the equatorial North Atlantic.

The evolution of the meridional mode event in 2009 was similar to that of a composite meridional mode

presented by Chiang et al. (2002). They showed that a negative meridional mode event, as occurred in 2009, is characterized by anomalous surface winds directed from the cold to the warm hemisphere together with an anomalous southward displacement of the ITCZ. The composite meridional mode in Chiang et al. (2002) peaks during February–May and is preceded by anomalously strong trade winds in the tropical North Atlantic during the preceding December–January, consistent with the event in 2009. Although the evolution of the 2009 event was similar to the composite evolution, there are also some important differences. First, there were warmer than normal SSTs in the equatorial and tropical South Atlantic during boreal winter 2008/09 coincident with the development of positive wind speed anomalies in the tropical North Atlantic. For the composite meridional mode, SSTs in the equatorial and South Atlantic are close to normal during the preceding December–January. Second, the cold SST anomalies in the tropical North Atlantic during 2009 were strongest in a band centered at about 5°N, whereas the composite meridional mode shows cold SST anomalies centered near 15°N. These two differences likely were responsible for the much stronger than normal meridional mode event in 2009 since both would tend to enhance the meridional SST gradient in the equatorial Atlantic, leading to stronger equatorial wind anomalies and associated positive wind evaporation–SST feedback.

The results from this study suggest that there may be positive coupled feedbacks between Ekman pumping anomalies north of the equator and the cross-equatorial SST gradient anomaly. If present, this feedback is likely to be strongest in the central and eastern equatorial Atlantic, where the mean thermocline is shallowest, and may act concurrently with positive wind evaporation–SST (WES) feedback in the western Atlantic (Chang et al. 1997; Xie 1999; Chang et al. 2000). For example, after cold SST anomalies developed north of the equator in January 2009, northwesterly anomalous surface winds developed, causing anomalous Ekman pumping, shoaling of the thermocline, and cooling through entrainment and vertical turbulent diffusion. The anomalous cooling intensified the cross-equatorial SST gradient anomaly, which would tend to generate stronger northwesterly wind anomalies.

The possibility of positive coupled wind–Ekman pumping–SST feedback was explored by Chang and Philander (1994) for the seasonal cycle in the eastern equatorial Pacific and Atlantic. They found evidence for such a positive feedback and showed that it is likely strongest within a few degrees of the equator, where the frictional term in the momentum balance is stronger than the Coriolis effect. Based on this theory, a positive meridional mode and associated cross-equatorial

southeasterly winds would generate Ekman pumping (i.e., upwelling) and cool SSTs along and south of the equator, enhancing southeasterly winds. The same would apply to cross-equatorial northwesterly winds, as occurred during the 2009 negative meridional mode event. The main difference between Chang and Philander's (1994) results and the events in 2009 is that Chang and Philander's model assumes that anomalies of the thermocline depth do not affect SST. In contrast, we found pronounced anomalous shoaling of the thermocline in the central and eastern equatorial North Atlantic during boreal spring 2009 that contributed to the observed anomalous cooling of SST. This potential coupling of thermocline depth to SST in the equatorial North Atlantic during meridional mode events would tend to enhance any positive wind–Ekman pumping–SST feedback relative to that predicted by Chang and Philander's (1994) model.

Both the WES feedback and potential Ekman pumping feedback are likely to be strongest in the boreal spring, when the thermocline is shallowest climatologically in the 2°–12°N band and surface winds are most responsive to anomalies of the meridional SST gradient (e.g., Chiang et al. 2002). Experiments with coupled models will be helpful for testing whether positive Ekman feedback is active and for clarifying the relative importance of Ekman pumping, surface heat fluxes, and air-sea coupling for generating SST anomalies in the equatorial North Atlantic. As the observational records from Argo and PIRATA expand, it will also be possible to determine the extent to which the mechanisms at play in 2009 can be invoked to describe SST variability in the equatorial North Atlantic in general.

**Acknowledgments.** We thank David Enfield, Semyon Grodsky, and two anonymous reviewers for helpful suggestions that improved the quality of this paper. The TropFlux product is developed as a collaboration between National Institute of Oceanography (Goa, India) and Institut Pierre-Simon Laplace (IPSL; Paris, France).

## APPENDIX

### Error Estimates

#### a. Satellite–Argo area averages

Here we describe the methodology used to estimate errors for each term in the mixed layer temperature equation (5). Errors in the rate of change of mixed layer temperature are due to uncertainties in TMI/AMSR-E SST. We have estimated these errors to be  $\pm 0.1^{\circ}\text{C}$ , based on the monthly RMS difference between TMI–AMSR-E SST and

temperature at a depth of 1 m from the PIRATA moorings at 4°N, 38°W and 4°N, 23°W during 2003–09.

Uncertainties in daily-averaged latent heat flux ( $Q_e$ ) and surface shortwave radiation (SWR) are  $\pm 20 \text{ W m}^{-2}$ , and for the net surface heat flux ( $Q_0$ ) a value of  $\pm 30 \text{ W m}^{-2}$  is used, following Kumar et al. (2011). These values are converted to monthly errors assuming an integral time scale (an estimate of the time period required to gain a new degree of freedom) of 3 days.

Errors in monthly Argo mixed layer depth (MLD),  $\Delta T$ , and  $Z_{20}$  are calculated as the standard error of all measurements in a given equatorial North Atlantic (ENA) subregion for a given month. Typical errors are  $\pm 5 \text{ m}$  for mixed layer depth,  $0.3^\circ\text{C}$  for  $\Delta T$ , and  $5 \text{ m}$  for  $Z_{20}$ .

Errors for each term in (5) averaged in each ENA subregion are calculated using the monthly errors for SST,  $Q_e$ ,  $Q_0$ , SWR, MLD,  $\Delta T$ , and  $Z_{20}$  and assuming the errors are uncorrelated in time. Errors for the ENA region are then calculated using the errors associated with each subregion, assuming two spatial degrees of freedom in the ENA region. The errors for the sum of the terms on the right-hand side of (5) and the observed change in SST are shown in Table 2.

### b. PIRATA moorings

Errors for each term in (6) are estimated using the methodology of Foltz and McPhaden (2009). Typical errors are 5–10 m for MLD and  $Z_{20}$ ,  $0.7^\circ\text{C month}^{-1}$  for latent heat flux,  $0.1^\circ\text{C month}^{-1}$  for sensible heat flux,  $0.1^\circ\text{C month}^{-1}$  for longwave radiation,  $0.9^\circ\text{C month}^{-1}$  for absorbed shortwave radiation, and  $1.4^\circ\text{C month}^{-1}$  for horizontal advection. Error estimates for shortwave radiation are likely underestimated at 12°N, 23°W since they do not include the effect of dust accumulation on the sensor (e.g., Foltz and McPhaden 2008). Visual inspection of the record at 12°N, 23°W did not reveal any obvious jumps in shortwave radiation immediately following sensor swaps, which generally indicates significant dust accumulation.

## REFERENCES

- Adler, R. F., and Coauthors, 2003: The version-2 Global Precipitation Climatology Project (GPCP) monthly precipitation analysis (1979–present). *J. Hydrometeor.*, **4**, 1147–1167.
- Bonjean, F., and G. S. E. Lagerloef, 2002: Diagnostic model and analysis of the surface currents in the tropical Pacific Ocean. *J. Phys. Oceanogr.*, **32**, 2938–2954.
- Bourlès, B., and Coauthors, 2008: The PIRATA program: History, accomplishments, and future directions. *Bull. Amer. Meteor. Soc.*, **89**, 1111–1125.
- Cane, M. A., 1979: The response of an equatorial ocean to simple wind stress patterns: I. Model formulation and analytic results. *J. Mar. Res.*, **37**, 233–252.
- Carton, J. A., and B. H. Huang, 1994: Warm events in the tropical Atlantic. *J. Phys. Oceanogr.*, **24**, 888–903.
- , X. H. Cao, B. S. Giese, and A. M. daSilva, 1996: Decadal and interannual SST variability in the tropical Atlantic Ocean. *J. Phys. Oceanogr.*, **26**, 1165–1175.
- Cayan, D. R., 1992: Latent and sensible heat flux anomalies over the northern oceans—driving the sea surface temperature. *J. Phys. Oceanogr.*, **22**, 859–881.
- Chang, P., and S. G. Philander, 1994: A coupled ocean–atmosphere instability of relevance to the seasonal cycle. *J. Atmos. Sci.*, **51**, 3627–3648.
- , L. Ji, and H. Li, 1997: A decadal climate variation in the tropical Atlantic Ocean from thermodynamic air–sea interactions. *Nature*, **385**, 516–518.
- , R. Saravanan, L. Ji, and G. C. Hegerl, 2000: The effect of local sea surface temperatures on atmospheric circulation over the tropical Atlantic sector. *J. Climate*, **13**, 2195–2216.
- , L. Ji, and R. Saravanan, 2001: A hybrid coupled model study of tropical Atlantic variability. *J. Climate*, **14**, 361–390.
- Chiang, J. C. H., Y. Kushnir, and A. Giannini, 2002: Deconstructing Atlantic intertropical convergence zone variability: Influence of the local cross-equatorial sea surface temperature gradient and remote forcing from the eastern equatorial Pacific. *J. Geophys. Res.*, **107**, 4004, doi:10.1029/2000JD000307.
- Czaja, A., P. Van der Vaart, and J. Marshall, 2002: A diagnostic study of the role of remote forcing in tropical Atlantic variability. *J. Climate*, **15**, 3280–3290.
- Doi, T., T. Tozuka, and T. Yamagata, 2010: The Atlantic meridional mode and its coupled variability with the Guinea Dome. *J. Climate*, **23**, 455–475.
- Enfield, D. B., and D. A. Mayer, 1997: Tropical Atlantic sea surface temperature variability and its relation to El Niño–Southern Oscillation. *J. Geophys. Res.*, **102**, 929–945.
- Fairall, C. W., E. F. Bradley, J. E. Hare, A. A. Grachev, and J. B. Edson, 2003: Bulk parameterization of air–sea fluxes: Updates and verification for the COARE algorithm. *J. Climate*, **16**, 571–591.
- Foltz, G. R., and M. J. McPhaden, 2006: The role of oceanic heat advection in the evolution of tropical North and South Atlantic SST anomalies. *J. Climate*, **19**, 6122–6138.
- , and —, 2008: Impact of Saharan dust on tropical North Atlantic SST. *J. Climate*, **21**, 5048–5060.
- , and —, 2009: Impact of barrier layer thickness on SST in the central tropical North Atlantic. *J. Climate*, **22**, 285–299.
- , and —, 2010a: Abrupt equatorial wave-induced cooling of the Atlantic cold tongue in 2009. *Geophys. Res. Lett.*, **37**, L24605, doi:10.1029/2010GL045522.
- , and —, 2010b: Interaction between the Atlantic meridional and Niño modes. *Geophys. Res. Lett.*, **37**, L18604, doi:10.1029/2010GL044001.
- , J. Vialard, B. P. Kumar, and M. J. McPhaden, 2010: Seasonal mixed layer heat balance of the southwestern tropical Indian Ocean. *J. Climate*, **23**, 947–965.
- Giannini, A., R. Saravanan, and P. Chang, 2003: Oceanic forcing of Sahel rainfall on interannual to interdecadal time scales. *Science*, **302**, 1027–1030.
- Gould, J., and Coauthors, 2004: Argo profiling floats bring new era of in situ ocean observations. *Eos, Trans. Amer. Geophys. Union*, **85**, doi:10.1029/2004EO190002.
- Hastenrath, S., and L. Greischar, 1993: Circulation mechanisms related to Northeast Brazil rainfall anomalies. *J. Geophys. Res.*, **98**, 5093–5102.
- Hayes, S. P., P. Chang, and M. J. McPhaden, 1991: Variability of the sea surface temperature in the eastern equatorial Pacific during 1986–88. *J. Geophys. Res.*, **96**, 10 553–10 566.

- Hu, Z. Z., and B. H. Huang, 2006: Physical processes associated with the tropical Atlantic SST meridional gradient. *J. Climate*, **19**, 5500–5518; Corrigendum, **20**, 4288.
- Huang, B. H., P. S. Schopf, and J. Shukla, 2004: Intrinsic ocean-atmosphere variability of the tropical Atlantic Ocean. *J. Climate*, **17**, 2058–2077.
- Kalnay, E., and Coauthors, 1996: The NCEP/NCAR 40-Year Reanalysis Project. *Bull. Amer. Meteor. Soc.*, **77**, 437–471.
- Kumar, B. P., J. Vialard, M. Lengaigne, V. S. N. Murty, and M. J. McPhaden, 2011: TropFlux: Air-sea fluxes for the global tropical oceans—Description and evaluation. *Climate Dyn.*, doi:10.1007/s00382-011-1115-0, in press.
- Lagerloef, G. S. E., G. T. Mitchum, R. B. Lukas, and P. P. Niiler, 1999: Tropical Pacific near-surface currents estimated from altimeter, wind, and drifter data. *J. Geophys. Res.*, **104**, 23 313–23 326.
- Lamb, P. J., 1978: Large-scale tropical Atlantic surface circulation patterns associated with sub-Saharan weather anomalies. *Tellus*, **30**, 240–251.
- Latif, M., N. Keenlyside, and J. Bader, 2007: Tropical sea surface temperature, vertical wind shear, and hurricane development. *Geophys. Res. Lett.*, **34**, L01710, doi:10.1029/2006GL027969.
- Lee, T., I. Fukumori, and B. Tang, 2004: Temperature advection: Internal versus external processes. *J. Phys. Oceanogr.*, **34**, 1936–1944.
- Liebmann, B., and C. A. Smith, 1996: Description of a complete (interpolated) outgoing longwave radiation dataset. *Bull. Amer. Meteor. Soc.*, **77**, 1275–1277.
- Lindzen, R. S., and S. Nigam, 1987: On the role of sea surface temperature gradients in forcing low-level winds and convergence in the tropics. *J. Atmos. Sci.*, **44**, 2418–2436.
- McPhaden, M. J., 1982: Variability in the central equatorial Indian Ocean. Part II: Oceanic heat and turbulent energy balance. *J. Mar. Res.*, **40**, 403–419.
- Nobre, C., and J. Shukla, 1996: Variations of sea surface temperature, wind stress, and rainfall over the tropical Atlantic and South America. *J. Climate*, **9**, 2464–2479.
- Reynolds, R. W., N. A. Rayner, T. M. Smith, D. C. Stokes, and W. Wang, 2002: An improved in situ and satellite SST analysis for climate. *J. Climate*, **15**, 1609–1625.
- Saravanan, R., and P. Chang, 2000: Interaction between tropical Atlantic variability and El Niño–Southern Oscillation. *J. Climate*, **13**, 2177–2194.
- Sun, B., L. Yu, and R. A. Weller, 2003: Comparisons of surface meteorology and turbulent heat fluxes over the Atlantic: NWP model analyses versus moored buoy observations. *J. Climate*, **16**, 679–695.
- Tanimoto, Y., and S. P. Xie, 2002: Interhemispheric decadal variations in SST, surface wind, heat flux, and cloud cover over the Atlantic Ocean. *J. Meteor. Soc. Japan*, **80**, 1199–1219.
- Wallace, J. M., and D. S. Gutzler, 1981: Teleconnections in the geopotential height field during the Northern Hemisphere winter. *Mon. Wea. Rev.*, **109**, 784–812.
- Wang, C. Z., D. B. Enfield, S.-K. Lee, and C. W. Landsea, 2006: Influences of the Atlantic warm pool on Western Hemisphere summer rainfall and Atlantic hurricanes. *J. Climate*, **19**, 3011–3028.
- Xie, S.-P., 1999: A dynamic ocean-atmosphere model of the tropical Atlantic decadal variability. *J. Climate*, **32**, 64–70.
- , and J. A. Carton, 2004: Tropical Atlantic variability: Patterns, mechanisms, and impacts. *Earth's Climate: The Ocean–Atmosphere Interaction*, Geophys. Monogr., Vol. 147, Amer. Geophys. Union, 121–142.
- Zhang, Y., W. B. Rossow, A. A. Lacis, V. Olnas, and M. I. Mishchenko, 2004: Calculation of radiative fluxes from the surface to top of atmosphere based on ISCCP and other global data sets: Refinements of the radiative transfer model and input data. *J. Geophys. Res.*, **109**, D19105, doi:10.1029/2003JD004457.